Kaolinitic Raw Materials for Ceramics

Subjects: Chemistry, Applied

Contributor: Christophe ENOCK EMBOM, Jean Aime Mbey

Eight kaolinitic materials from the Lokoundje River at Kribi were sampled and investigated for their physical, chemical, mineralogical and thermal characteristics in order to evaluate their potential suitability as raw materials in ceramics. The Lokoundje kaolinitic materials are clayey to silty clayey and are predominantly composed of kaolinite and quartz. The alkali (Na2O + K2O) content ranges between 1 and 2.5 wt.%; these low values do not favor vitrification of the ceramics but may be improved through flux amendment. The presence of goethite in some samples limits their utilization in white ceramics. The minerals content, color, metallic sound, cohesion, linear shrinkage, flexural strength, bulk density, water absorption and microstructure were determined. The XRD data reveal that kaolinite and goethite were transformed, respectively, into mullite and hematite. The colors of the fired products are characteristic of their mineral assemblage. The metallic sound is indicative of low vitrification which is confirmed by the presence of cracks due to low flux contents. The cohesion is good to very good, due to the abundance of kaolinite. The physicomechanical properties increase with temperature as well as densification. The geochemical data show that the Lokoundje alluvial clays are suitable for the manufacture of white stoneware tiles.

Keywords: Kribi ; alluvial clays ; kaolinite ; valorization ; low mullitization ; white stoneware tiles

1. Introduction

The investigation of clays as raw materials for ceramic industry has been a long-standing research activity spanning over many centuries. Clays mineral are used in traditional ceramics for fired bricks, stoneware or porcelain [1][2]. The interest human societies have in clay materials is due to the several varieties of applications [3]. Clay materials are used to promote sustainable development in many countries due to their low cost and availability for use in the building industry [3]. Kaolin occurs as a ubiquitous raw material with many applications, such as filler in paper, plastics, paints, and rubber. In view of promoting the quality used of available clay resources around the world, many studies are being conducted on their valorization in various applications, such as cementitious-product making [4][5], water treatment [6][7][8][9][10], pollution remediation [11][12], earthen ceramic production [13][14][15], and polymer–clay composites [16][17]. The present study focused on the evaluation of the potentiality of alluvial kaolinite from Kribi as a potential raw material for the production of earthen ceramics. The testing of the material from this region is motivated by the deposit size, which may allow a large-scale production if the material properties are favorable. To this end, the chosen samples were subjected to chemical, mineralogical, physical, and textural analyses to determine their properties, as well as performance evaluation of the fired specimens.

2. Thermal Behavior and XRD Mineralogical Evolution in Fired Samples

The thermal analyses (TGA-DTG) measurements are reported in **Figure 1**. The thermal analyses show three mass losses: the first loss occurs around 60–66 °C and corresponds to the loss of adsorbed water [18][19][20]. The second mass loss at 241–252 °C is associated with the conversion of goethite into hematite, and the last one at 489–492 °C is related to the dehydroxylation of kaolinite [21]. The goethite to hematite conversions confirm that iron is mainly present in form of goethite and that this will probably lead to a reddish color in the fired sample. The variation in the temperature of the last mass loss (489–492 °C) is associated with the crystallinity difference of the kaolinite [18]. As previously reported, FTIR revealed that kaolinite has a high degree of disorder, characteristic of several alluvial environments [22][23]. The intensity of the dehydroxylation peaks (489–492 °C) is coherent with kaolinite-rich materials and the associated mass loss varied between 14% and 18%; these values are consistent with the theoretical weight loss from the kaolinite ideal formula of 14%.

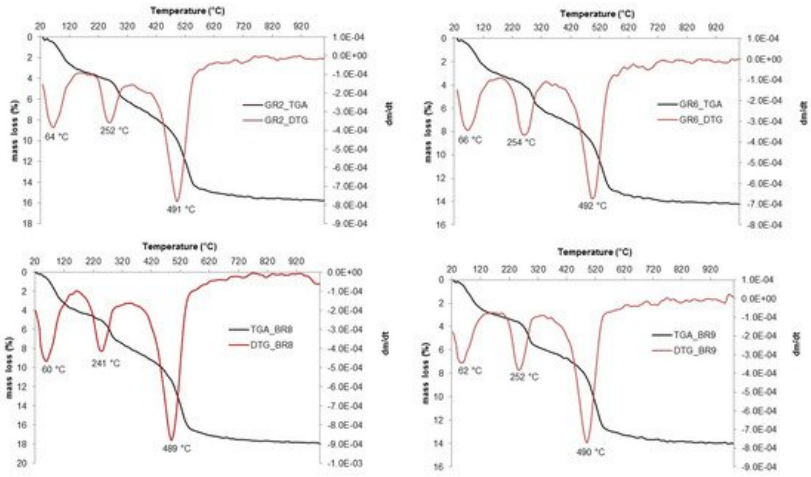

Figure 1. TG-DSC of Lokoundje alluvial materials.

The color of the specimens is variable as a function of the initial color of the raw materials, as well as their mineral compositions. The pale brown sample becomes light red; the light gray becomes dark red or white; and brownish gray becomes pink (**Table 1**, **Figure 2**). This is associated with the fact that, during the sintering process, goethite is converted into hematite, which justifies the reddish and brownish colors, as suggested by the thermal analyses. The whitish color is mainly the mark of a sample with low iron content [24]. The sound of the fired products is metallic (**Table 1**), which is indicative of vitrification that accounts for improved sintering. The cohesion of the fired products is good to very good (**Table 1**). The weak cohesion of sample BR9 may be related to the proportion of coarse particles. The mineral assemblage of the fired products, from XRD analyses (**Figure 3**), is made of quartz, mullite, rutile and hematite. Mullite is developed from the spinel phase, which is formed from the demixion of metakaolin that is formed after kaolinite dehydroxylation [25][26]. The illite peak, although low, is still observable in the products fired at 800 °C and 900 °C. Illite dehydroxylation evolved from 300 °C to 700 °C. The relic illite structure breaks down between 700 °C and 850 °C, leading to a liquid phase formation, which crystallizes to form a spinel which crystalizes until it changes to mullite above 1100 °C [27]. In the particular case of these materials, the mullitization peaks, observed from 800 °C, are associated with the structural disorder of the clay minerals present in the raw samples.

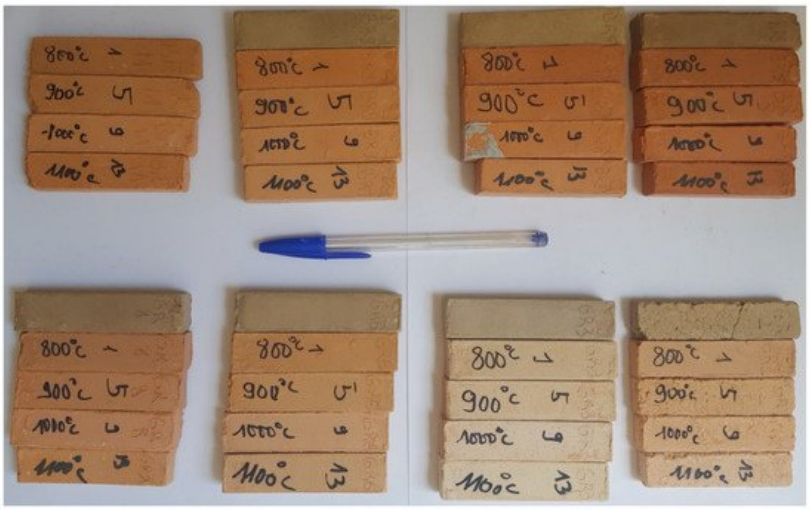

Figure 2. Pictures of specimens.

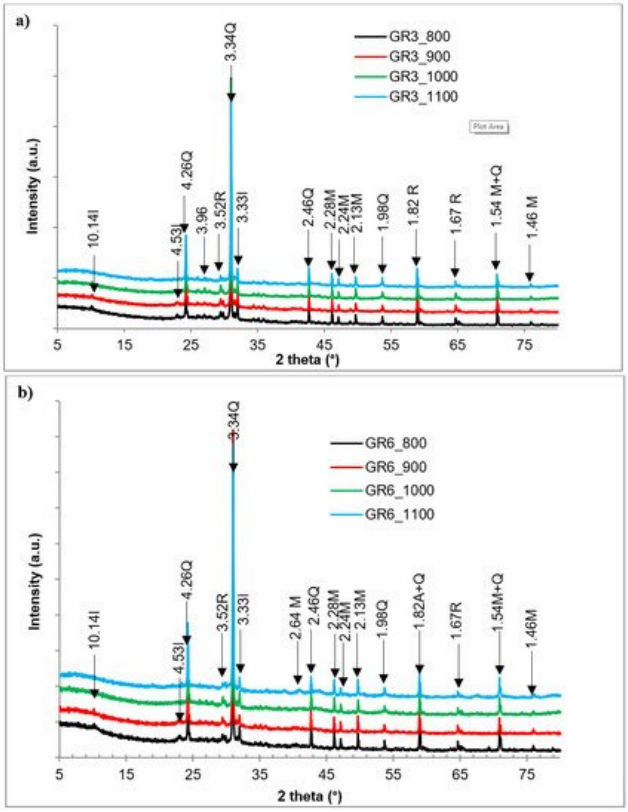

Figure 3. X-ray patterns of the clay sintered at different temperatures: (**a**) GR3 sample; (**b**) GR6 sample; I: illite; Q: quartz; M: mullite; R: rutile; He: hematite.

Table 1. Color, sound, and cohesion of the raw materials and fired products.

Sample	Temperature (°C)	Color	Sound	Cohesion
BR-5	25	Pale brown	-	-
	800	Light red	Metallic	Good
	900	Light red	Metallic	Good
	1000	Light red	Metallic	Very good
	1100	Light red	Metallic	Very good
BR-8	25	Pale brown	-	-
	800	Reddish yellow	Metallic	Good
	900	Reddish yellow	Metallic	Good
	1000	Light red	Metallic	Good
	1100	Light red	Metallic	Very good
BR-9	25	Light gray	-	-
	800	Reddish yellow	Metallic	Weak
	900	Light red	Metallic	Average
	1000	Red	Metallic	Average
	1100	Dark red	Metallic	Good
BR-11	25	Reddish yellow	-	-
	800	Reddish yellow	Metallic	Good
	900	Reddish yellow	Metallic	Good
	1000	Reddish yellow	Metallic	Very good
	1100	Light red	Metallic	Good

Sample	Temperature (°C)	Color	Sound	Cohesion
GR-2	25	Brownish gray	-	-
	800	Reddish brown	Metallic	Good
	900	Pink	Metallic	Good
	1000	Pink	Metallic	Very good
	1100	Pink	Metallic	Good
GR-3	25	Light gray	-	-
	800	Pinkish white	Metallic	Good
	900	Pinkish white	Metallic	Very good
	1000	Pinkish white	Metallic	Very good
	1100	White	Metallic	Good
GR-6	25	Brownish gray	-	-
	800	Reddish yellow	Metallic	Good
	900	Reddish yellow	Metallic	Good
	1000	Pink	Metallic	Very good
	1100	Pink	Metallic	Very good
GR-8	25	Pale brown	-	-
	800	Light red	Metallic	Good
	900	Light red	Metallic	Good
	1000	Light red	Metallic	Very good
	1100	Light red	Metallic	Very good

3. Technological Characterization of Fired Products

The linear shrinkage increases with the firing temperature (**Figure 4**a). The loss of weight varies between 5 and 17%. The values are almost constant for all the firing temperatures (**Figure 4**b). This may be justified by the low organic contamination of the samples or to the predominance of clay minerals.

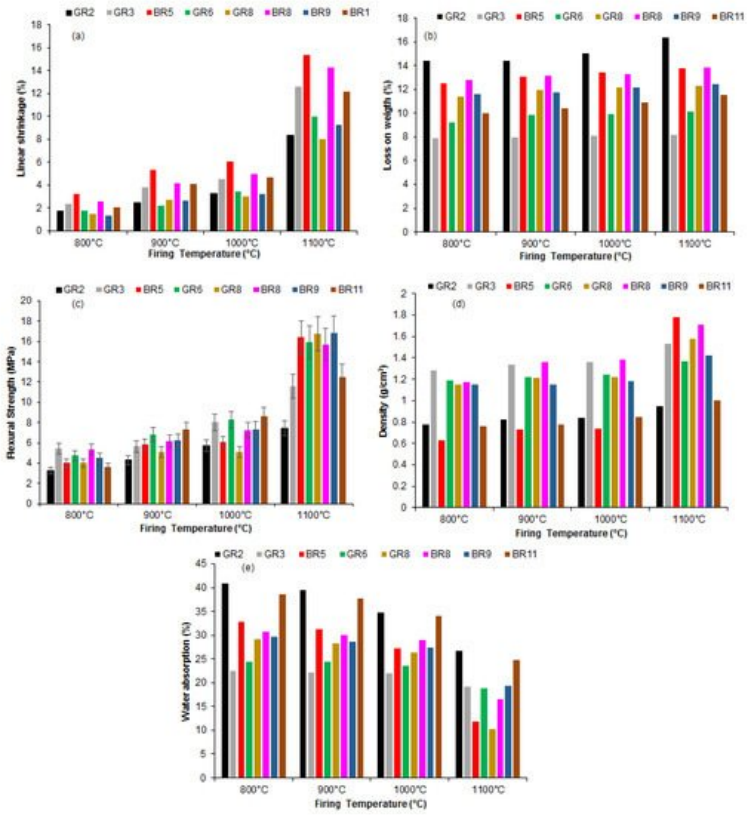

Figure 4. Influence of firing temperature on the physical and mechanical properties of Kribi clays: (**a**) linear shrinkage; (**b**) weight loss; (**c**) flexural strength; (**d**) bulk density and (**e**) water adsorption.

The flexural strength increases with the firing temperature because of an increase in densification (**Figure 4**c). This densification is supported by the XRD patterns, in which an increase in mullite formation with temperature is noticeable. The highest value obtained was 15.75 MPa for sample BR5 fired at 1100 °C. For all other samples, the highest value of flexural strength was reached at 1100 °C (**Figure 4**c). This can be explained by the high Al_2O_3 content [28] and/or the increased formation of a dense phase, such as mullite during sintering [29]. The bulk density (**Figure 4**d) followed the same trend as the flexural strength, which was consistent with the proposed increase in density upon firing, because of dense phase formation. Between 800 and 1000 °C, the bulk density is almost constant. This may be due to the similar mineralogical composition of the samples, in which the main dense phases are quartz and a primary mullite from 1000 °C (**Figure 3**). The density of the BR5 sample was also the highest among the series. Given that its clay size fraction, from particle size analyses, was the highest (76%) for the GR2 sample, then the mullite formation from sintering was higher in these samples compared to others. The difference reached in the flexural strength was probably due to crystallinity differences, which may affect the kinetics of mullite formation.

The decrease in the water absorption (**Figure 4**e) is in agreement with the change in the flexural strength and the bulk density as a result of improved sintering. These values were considerably reduced to less than 20% at 1100 °C, except for in two samples (GR-2 and BR-11), probably because of a glassy phase formation that diffuses between the grains, causing pore enclosure. The water absorption was less than 25%, indicating that these clayey materials can be of use for tile manufacturing. At 800 °C, the sintering was not sufficient to improve densification, which explains the high level of water adsorption.

4. Microstructure

An examination of the microstructure under SEM reveals the presence of several cracks at 1000 °C (**Figure 5**a–e,g) and rounded pores at 1100 °C (**Figure 5**f,h). The presence of cracks confirms low densification during sintering at temperatures <1100 °C. The abundance of alumina, the low flux contents, as well as the low Fe_2O_3 contents (**Table 1**) can confirm this behavior [30]. Additionally, at 1000 °C, the densification is still poor as mullite formation is still limited (**Figure 5**a,b). The low densification might also be linked to the low mullite formation. As reported in [31], before 1100 °C, XRD peaks associated to mullite more often account for the spinel that will crystalize as mullite. The mullite needle starts to be observable from 1100 °C; at this temperature, the strength is relatively high.

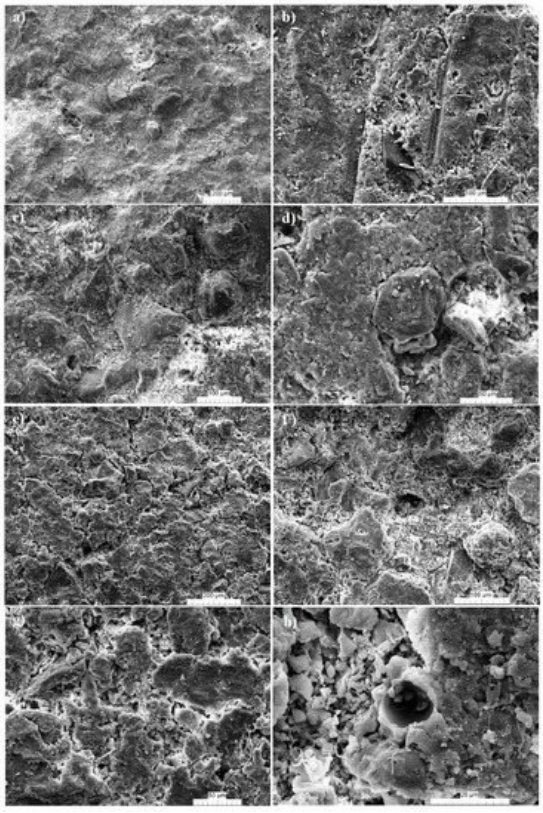

Figure 5. SEM images of the fired products from the Kribi alluvial clays: Gr-3 sample at 1000 °C (**a**–**d**); Gr-3 sample at 1100 °C (**e**–**h**).

References

1. Bergaya, F.; Theng, B.K.G.; Lagaly, G. Clays in industry. In Developments in Clay Sciences. Bergaya, Theng, and Lagaly, 1st ed.; Elsevier: Amsterdam, The Netherlands, 2006; ISBN 13-978-0-08-044183-2.
2. Anglisano, A.; Casas, L.; Anglisano, M.; Queralt, I. Application of Supervised Machine-Learning Methods for Attesting Provenance in Catalan Traditional Pottery Industry. Minerals 2020, 10, 8.
3. Ekosse, E.G.I. Kaolin deposits and occurrences in Africa: Geology, mineralogy and utilization. Appl. Clay Sci. 2010, 50, 212–236.
4. Khelifi, H.; Perrot, A.; Lecompte, T.; Ausias, G. Design of clay/cement mixtures for extruded building products. Mater. Struct. 2013, 46, 999–1010.
5. Tchakouté, H.K.; Rüscher, C.; Hinsch, H.M.; Djobo, J.N.Y.; Kamseu, E.; Leonelli, C. Utilization of sodium waterglass from sugar cane bagasse ash as a new alternative hardener for producing metakaolin-based geopolymer cement. Geochemistry 2017, 77, 257–266.
6. Cripps, H.R.; Isaias, N.P.; Jowet, A. The use of clays as an aid to water purification. Hydrometallurgy 1976, 1, 373–387.
7. Beall, G.W. The use of organo-clays in water treatment. Appl. Clay Sci. 2003, 24, 11–20.
8. Belibi Belibi, P.; Nguemtchouin, M.M.G.; Rivallin, M.; Ndi Nsami, J.; Sielechi, J.; Cerneaux, S.; Ngassoum, M.B.; Cretin, M. Microfiltration ceramic membranes from local Cameroonian clay applicable to water treatment. Ceram. Int. 2015, 41, 2752–2759.
9. Djoufac, W.E.; Siéwé, J.M.; Njopwouo, D. A fixed-bed column for phosphate removal from aqueous solutions using an andosol-bagasse mixture. J. Environ. Manag. 2015, 151, 450–460.
10. Siéwé, J.M.; Djoufac, W.E.; Djomgoue, P.; Njopwouo, D. Activation of clay surface of Bambouto's andosol (Cameroon) with phosphate ions. Application for copper fixation in aqueous solution. Appl. Clay Sci. 2015, 114, 31–39.
11. Zhang, G.; Lin, Y.; Wang, M. Remediation of copper polluted red soils with clay materials. J. Environ. Sci. 2011, 23, 461–467.
12. Yuan, G.D.; Theng, B.K.G.; Churchman, G.J.; Gates, W.P. Clays and Clay Minerals for Pollution Control. Developments in Clay Science; Chapter 5.1; Elsevier: Amsterdam, The Netherlands, 2013; pp. 587–644.
13. Tite, M.S. Ceramic production, provenance and use—A review. Archaeometry 2008, 50, 216–231.
14. Fadil-Djenabou, S.; Ndjigui, P.-D.; Mbey, J.A. Morphological and physicochemical characterization of Ngaye alluvial clays (Northern Cameroon) and assessment of its suitability in ceramic production. J. Asian Ceram. Soc. 2015, 3, 50–58.
15. Tsozue, D.; Nzeukou, N.A.; Mache, J.R.; Loweh, S.; Fagel, N. Mineralogical, physico-chemical and technological characterization of clays from Maroua (Far-North Cameroon) for use in ceramic bricks production. J. Build. Eng. 2017, 11, 17–24.
16. Mbey, J.A.; Thomas, F.; Ngally Sabouang, C.J.; Liboum, N.D. An insight on the weakening of the interlayer bonds in a Cameroonian kaolinite through DMSO intercalation. Appl. Clay Sci. 2013, 83, 327–335.
17. Mbey, J.A.; Hoppe, S.; Thomas, F. Cassava starch-kaolinite composite films. Thermal and mechanical properties related to filler-matrix interactions. Polym. Compos. 2015, 36, 184–191.
18. Hu, P.; Yang, H. Insight into the physicochemical aspects of kaolin with different morphologies. Appl. Clay Sci. 2013, 74, 58–65.
19. Mache, J.R.; Signing, P.; Njoya, A.; Kunyukubundo, F.; Mbey, J.A.; Njopwouo, D. Smectite clay from the Sabga deposit (Cameroon): Mineralogical and physicochemical properties. Clay Miner. 2013, 48, 499–512.
20. Ndjigui, P.-D.; Mbey, J.A.; Nzeukou, N.A. Mineralogical, physical and mechanical features of ceramic products of the alluvial clastic clays from the Ngog-Lituba region, Southern Cameroon. J. Build. Eng. 2016, 5, 151–157.
21. Nzeukou, N.A.; Fagel, N.; Njoya, A.; Kamgang Beyala, V.; Eko Medjo, R.; Melo Chinje, U. Mineralogy and physico-chemical properties of alluvial clays from Sanaga valley (Center, Cameroon): Suitability for ceramic application. Appl. Clay Sci. 2013, 83, 238–243.
22. Ndjigui, P.-D.; Onana, V.L.; Sababa, E.; Bayiga, E.C. Mineralogy and geochemistry of the Lokoundje alluvial clays from the Kribi deposits, Cameroon Atlantic coast: Implications for their origin and depositional environment. J. Afri. Earth Sci.

2018, 143, 102–117.

23. Ndjigui, P.-D.; Ebah Abeng, S.A.; Ekomane, E.; Nzeukou, N.A.; Ngo Mandeng, F.S.; Lindjeck, M.M. Mineralogy and geochemistry of pseudogley soils and recent alluvial clastic sediments in the Ngog-Lituba region, Southern Cameroon: An implication to their genesis. J. Afr. Earth Sci. 2015, 108, 1–14.
24. Sonuparlak, B.; Sarikaya, M.; Aksay, I.A. Spinel phase formation during the 980°C exothermic reaction in the kaolinite-to-mullite reaction series. J. Am. Ceram. Soc. 1987, 70, 837–842.
25. Carbajal, L.; Rubio-Marcos, F.; Bengochea, M.A.; Fernandez, J.F. Properties related phase evolution in porcelain ceramics. J. Eur. Ceram. Soc. 2007, 27, 4065–4069.
26. Njoya, D.; Hajjaji, M.; Baçaoui, A.; Njopwouo, D. Microstructural characterization and influence of manufacturing parameters on technological properties of vitreous ceramic materials. Mater. Charact. 2010, 61, 289–295.
27. Caspar, J.; McConville, C.J.; Lee, W.E. Microstructural development on firing illite and smectite clays compared with that in kaolinite. J. Am. Ceram. Soc. 2005, 88, 2267–2276.
28. Mehta, S.N.; Sahu, K.P.; Tripathi, P.; Pyare, R.; Majhi, R.M. Influence of alumina and silica addition on the physico-mechanical and dielectric behavior of ceramic porcelain insulator at high sintering temperature. Bol. Soc. Española Cerámica Vidr. 2018, 57, 151–159.
29. Chen, C.Y.; Lan, G.S.; Tan, W.H. Microstructural evolution of mullite during the sintering of kaolin powder compacts. Ceram. Int. 2006, 26, 715–720.
30. Roudouane, H.T.; Mbey, J.A.; Bayiga, E.C.; Ndjigui, P.-D. Characterization and application tests of kaolinite clays from Aboudeia (southeastern Chad) in fired bricks making. Sci. Afr. 2020, 7, e00294.
31. Behera, P.S.; Bhattacharyya, S. Effect of different alumina sources on phase formation and densification of single-phase mullite ceramic–Reference clay alumina system. Mater. Today Com. 2021, 26, 101818.